


# Tailoring Magnetic Properties and Suppressing Anisotropy in Permalloy Films by Deposition in a Rotating Magnetic Field

Olga Lozhkina<sup>1</sup>, Fabian Kammerbauer<sup>1</sup>, Maria-Andromachi Syskaki<sup>1,2</sup>,  
Aravind Puthirath Balan<sup>1</sup>, Pascal Krautscheid<sup>1</sup>, Mehran Vafaei Khanjani<sup>1</sup>, Jan Kubik<sup>3</sup>,  
Stephen O'Brien<sup>3</sup>, Robert M. Reeve<sup>1</sup>, Gerhard Jakob<sup>1</sup>, Robert Frömter<sup>1,\*</sup> and Mathias Kläui<sup>1</sup>

<sup>1</sup>*Institute of Physics, Johannes Gutenberg University Mainz, Mainz 55099, Germany*

<sup>2</sup>*Singulus Technologies AG, Kahl am Main 63796, Germany*

<sup>3</sup>*Analog Devices, Limerick V94 RT99, Ireland*

 (Received 9 June 2022; revised 13 December 2022; accepted 2 June 2023; published 12 July 2023)

We investigate the optimal deposition conditions for permalloy ( $\text{Ni}_{81}\text{Fe}_{19}$ ) thin films fabricated via magnetron sputtering to achieve soft magnetic films for magnetoresistive sensing applications. The films are grown with different deposition techniques such as sputtering and molecular-beam epitaxy and parameters, including varying inert gas pressure and deposition power, and with different magnetic fields applied during the growth. Our approach enables sputtering of permalloy films with low coercivity while keeping high anisotropic magnetoresistance values. We develop a robust method to characterize the intrinsic magnetic anisotropy of the films that is not dominated by local defects and we demonstrate the possibility of magnetic anisotropy suppression via implementing a rotating magnetic field during sputtering.

DOI: [10.1103/PhysRevApplied.20.014021](https://doi.org/10.1103/PhysRevApplied.20.014021)

## I. INTRODUCTION

Permalloy ( $\text{Ni}_{75 \leq x \leq 82}\text{Fe}_{100-x}$ , Py) is an archetypal soft magnetic material [1] that possesses highly desirable properties such as extremely low magnetostriction, low coercivity, and vanishingly low magnetic anisotropy, making it attractive for a vast range of applications [2–9], which in turn demand easy tailoring of magnetic and electric properties. Thin films of permalloy are in-plane magnetized by their shape anisotropy but due to nonideal growth conditions, they usually exhibit an additional slight and possibly detrimental uniaxial in-plane anisotropic behavior. The coercivity and anisotropy of permalloy employed in low-field magnetic sensors, magnetic domain-wall logic, and memory devices should be as low as possible [10]. Low anisotropy and coercivity of permalloy is highly desirable for anisotropic magnetoresistance (AMR) sensors [11], which are of high interest for detecting and responding to external magnetic fields. AMR sensors are in high demand in areas where high sensitivity and flexibility of design are required; in particular, they can be used in wearable electronics for navigation, medical diagnosis, and health monitoring [12].

Py films used in industrial magnetoresistive devices are in most cases prepared by magnetron sputtering due to its high deposition rates, stability, flexibility in terms of

materials, achievable film thicknesses down to the sub-nanometer range, and the variety of controllable parameters, such as the plasma power, chamber pressure, sputtering angle, and deposition temperature. The permalloy properties to be tailored are the magnetic anisotropy [2,3,13,14], the coercivity [15,16], the exchange stiffness [17], and the damping constant [18–20]. Among the reported approaches are modifications of the composition (varying the nickel-to-iron ratio [14,21–23] or doping with transition [24], noble [20,24], and rare-earth [18,25] metals), material-stack variations [26–29] to modify the permalloy texture and avoid magnetically “dead” interfacial layers, optimization of the deposition [10,16,30,31] and annealing parameters [13,17], including field annealing [13], tilting the target [14,15,32], applying external fields during deposition [14,32,33], and the use of textured substrates [34–36] to promote anisotropy. Even though the material has been widely investigated for several decades, the origins of the different sources of anisotropy, including magnetocrystalline and growth-condition-induced anisotropies, are still a topic of intense discussion. Very early theories describe the crystalline anisotropy of permalloy via a simple vector sum of separate atomic moments [37], while recent studies consider atomic orbital hybridization in a variable chemical environment [38] and the associated charge redistribution [22]. The properties of permalloy can be significantly modified via field annealing but the mechanism of the effect is still being discussed. Various mechanisms resulting in uniaxial anisotropy in permalloy have

\*froemter@uni-mainz.de

been proposed, including Fe-Fe pair ordering effects [39], magnetostrictive contributions [40], and defects including vacancies, contaminants, and grain boundaries [41]. A recent study has found that the electrical resistivity of polycrystalline permalloy films is higher along the hard-axis direction than along the easy axis, which is in agreement with proposals that directional order can induce magnetic anisotropy in permalloy [33,42].

In addition to inducing anisotropy, studies have also investigated ways to suppress it: while permalloy films that are magnetically shielded during deposition still demonstrate a residual anisotropy [43], annealing in a rotating field is reported to fully suppress the anisotropy but is accompanied by an increase in the film coercivity [13,32]. Rotating the sample during deposition with respect to a tilted target drastically decreases both the coercivity and the anisotropy but only down to a certain plateau [33]. Finally, Py deposition at normal incidence in a rotating external field of 3 mT has been reported to result in isotropic properties when averaging over the entire film [32]; however, these films still exhibit anisotropy on a local scale, as can be concluded from the observation of magnetization ripples on a scale of 100  $\mu\text{m}$ .

All the above-mentioned approaches to the minimization of magnetic anisotropy rely on obtaining polycrystalline samples with a random orientation of crystallites, so that the local anisotropy averages out and the samples do not exhibit a net anisotropy [44,45]. However, fcc metals have a tendency to develop a (111) texture to minimize the surface energy, resulting in an intrinsic compressive stress due to the incorporation of surface atoms in the film caused by the high adatom energy [46]; this is also linked to a higher density and lower roughness and coercivity of the resulting films [15,31,47].

To summarize, a range of different factors impact the anisotropy of thin polycrystalline permalloy films and while the anisotropy of permalloy can be reduced, residual sources of anisotropy often remain, which can be detrimental for device performance, calling for further approaches to growth optimization. Furthermore, it is of paramount importance that robust techniques are established that can reliably benchmark the influence of varied deposition conditions on the film quality. Since extended thin films frequently contain macroscopic defects that occur randomly and are not necessarily directly related to the specific growth conditions, it is vital that such films are characterized in such a manner that the properties are not dominated by such extrinsic random defects but, rather, reflect the intrinsic properties of the varied deposition parameters. This approach can also be of interest for optimizing the growth conditions and analyzing the magnetic properties of soft magnetic films other than permalloy.

In this study, we prepare sets of thin Py films exhibiting in-plane magnetization with varied deposition

methods and parameters and investigate them by analysis techniques that probe the films both globally and locally. In addition, we employ lithographic patterning in order to isolate and distinguish the impact of individual sparsely distributed defects. In this manner, we develop an approach to robustly determine the film properties, so that we can reliably extract the influence of the growth procedure, independent of the presence of random macroscopic defects in the films that can otherwise dominate the properties. We then employ this approach to investigate various methods to reduce the coercivity and effectively control the anisotropy of the deposited films, in particular via the application of rotating magnetic fields during growth. This approach can be of interest for optimizing the growth conditions and analyzing the magnetic properties of various thin in-plane magnetic films.

## II. METHODS

Several sets of samples are produced by room-temperature dc magnetron sputtering in a Singulus Rotaris sputtering system using 10-cm-diameter material targets provided by Singulus on  $1 \times 1 \text{ cm}^2$  thermally oxidized (001) p-doped silicon substrates with a 100-nm oxide layer placed close to the rotational axis of the round 8-in.-diameter sample holder. Single deposition parameters are systematically varied while keeping the other ones fixed (deposition power in the range 200–1200 W, chamber pressure in the range  $4 \times 10^{-3}$ – $6 \times 10^{-3}$  mbar, or different applied magnetic field protocols).

In order to increase the AMR, which is important for sensing applications, a  $\text{Ni}_{47}\text{Cr}_{42}\text{Fe}_{11}$  seed layer is used, which also drastically improves the (111) texture of the films [48]. The complete material stack includes a 4-nm  $\text{Ni}_{47}\text{Cr}_{42}\text{Fe}_{11}$  seed layer, on top of which 30 nm of Py ( $\text{Ni}_{81}\text{Fe}_{19}$ ) is deposited—sufficient to provide a measurable change of the magnetic parameters for the different samples and to minimize the impact of interfacial effects such as intermixing that may dominate the properties of thinner films. Finally, a 4-nm Ta capping layer is deposited to prevent oxidation. The  $\text{Ni}_{47}\text{Cr}_{42}\text{Fe}_{11}$  and Ta layers are in all cases deposited under the same conditions (800 W and  $P_{\text{Ar}} = (3.6 \pm 0.3) \times 10^{-3}$  mbar for the  $\text{Ni}_{47}\text{Cr}_{42}\text{Fe}_{11}$  seed layer and 200 W and  $P_{\text{Ar}} = (3.5 \pm 0.2) \times 10^{-3}$  mbar for the Ta capping), with all layer thicknesses controlled by x-ray reflectometry (XRR).

Two different field protocols are investigated, either a so-called “aligning” magnetic field (AMF) that is fixed in space with respect to the rotating sample coordinate frame or a “rotating” magnetic field (RMF) that is fixed in the laboratory frame and therefore rotates with respect to the frame of reference of the film. While sputtering the Py and  $\text{Ni}_{47}\text{Cr}_{42}\text{Fe}_{11}$  films, rotating or aligning magnetic fields up to 5 mT are generated by four pairs of sinusoidally commutated solenoids placed in vacuum around the sample

holder. A third set of samples is prepared without applying an additional magnetic field (zero magnetic field, ZMF).

The deposition tilt is  $14^\circ$  with respect to the substrate normal and the target-to-substrate distance is 20 cm (Fig. 1). During deposition, the sample stage is rotated around its axis at a frequency of 1 Hz to provide uniformly thick films, to remove the influence of static background magnetic fields such as that of the Earth and the stray field of the cathode magnets, as well as to avoid self-shadowing [49].

Another set of samples is deposited by thermal evaporation in an ultrahigh-vacuum (UHV) molecular-beam-epitaxy chamber on the same substrates, cooled down to liquid-nitrogen temperatures (no seed layer, 52 nm of Py capped with 4 nm of gold) or at room temperature (25 nm of permalloy capped with 4 nm of gold). Here, the Py evaporator is tilted by  $5^\circ$  with respect to the substrate normal.

The magnetic properties of the prepared samples are investigated by both full-field magneto-optical Kerr-effect (MOKE) microscopy utilizing polarized light from a light-emitting diode (LED) (field of view  $340 \times 450 \mu\text{m}^2$ ) and vibrating sample magnetometry (VSM). For investigating the anisotropy, magnetic hysteresis loops are recorded for different in-plane rotation angles of the sample with respect to the external magnetic field direction using a step size ranging from  $5^\circ$  to  $15^\circ$ . To determine the directions of the easy and hard axes, the remanent magnetization versus angle plot is fitted with a function representing the modified Stoner-Wohlfarth model  $a|\cos(\alpha + x)| + c$ ,

where  $a$  is a normalization coefficient,  $\alpha$  is the rotation angle with respect to the external probing magnetic field, and  $x$  is the easy-axis direction [Figs. 2(a)–2(c)]. The anisotropy constant is calculated as the difference between  $M_s H_s - \frac{\int_{-H_s}^0 M_{\text{asc}} dH + \int_0^{H_s} M_{\text{desc}} dH}{2}$  for easy- and hard-axis hysteresis loops [50–52], where  $M_s$  is the saturation magnetization,  $M_{\text{asc}}(H)$  and  $M_{\text{desc}}(H)$  are the ascending and descending hysteresis-loop branches, and  $H_s$  is an arbitrarily chosen magnetic field value that needs to be at the level of, or higher than, the saturation field [Fig. 2(d)].

The roughness and average particle size of the samples are measured by atomic force microscopy (AFM), XRR, and x-ray diffraction (XRD). The average crystallite size is obtained using the Scherrer formula to describe the broadening of the Py  $\langle 111 \rangle$  XRD peak.

Subsequent patterning of the films into a hexagonal lattice ( $5 \times 5 \text{ mm}$ ) of disks with  $80\text{-}\mu\text{m}$  diameter and  $10\text{-}\mu\text{m}$  spacing is performed using near-ultraviolet photolithography and ma-P 1215 positive photoresist, which requires 30 s of soft baking at  $90^\circ\text{C}$ , followed by Ar ion-beam etching at 300 V.

### III. RESULTS

A first set of Py films is sputtered at room temperature with different adatom energies by varying the sputtering power and chamber pressure, using an external in-plane RMF of 5 mT. For samples with varied sputtering power, the chamber pressure is fixed at  $4 \times 10^{-3}$  mbar and

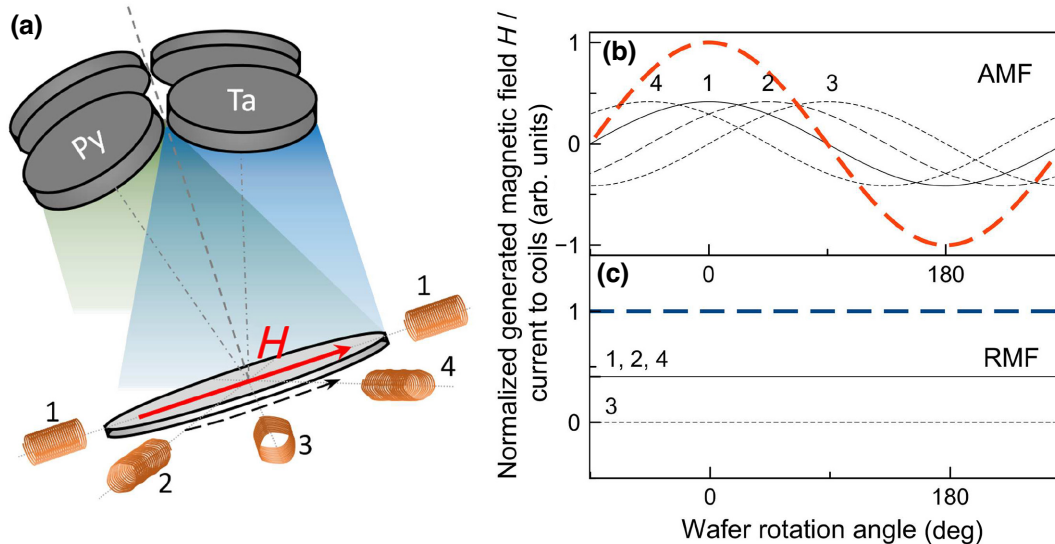


FIG. 1. (a) A schematic illustration of the deposition geometry in the Singulus Rotaris sputtering chamber that is used for the permalloy-thin-film deposition. The sample is placed on a rotating holder and four pairs of coils (1–4) are fixed in space in the plane of the holder to generate a magnetic field that is either static and thus rotating in the reference frame of the sample (RMF) or synchronized with the rotation of the sample and thus constant (aligning) in the frame of the sample (AMF). (b),(c) Plots of the currents applied to each of the four coil pairs and the resulting magnetic field at the sample position in the fixed laboratory frame as a function of the sample rotation angle, under (b) AMF growth conditions and (c) RMF growth conditions.

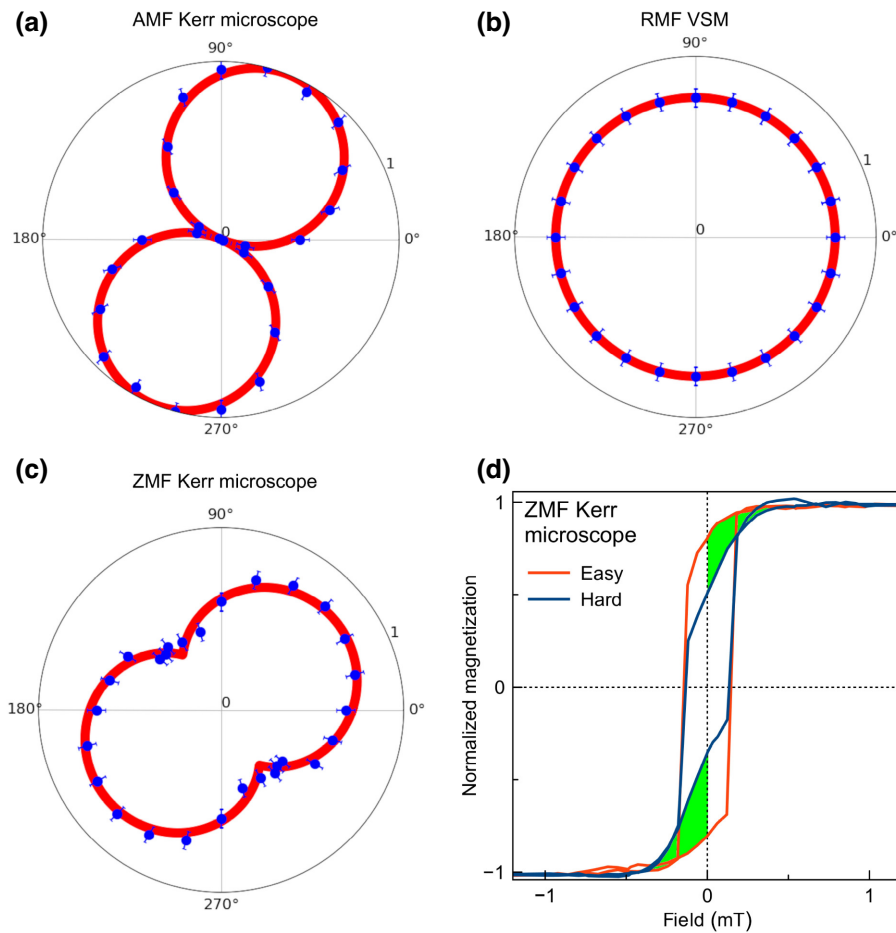


FIG. 2. (a)–(c) Exemplary angular dependencies of the normalized remanent magnetization measured using Kerr microscopy or VSM (blue dots), along with the corresponding fits (red curves) using the modified Stoner-Wohlfarth model to determine the easy- and hard-axis directions. The graphs are scaled from zero to 1. (d) The easy- and hard-axis hysteresis loops from the data set in (c), plotted with an area marked in green that represents the anisotropy constant  $\times \frac{2}{M_s}$  as evaluated using the area-integration method.

for samples with varied chamber pressure, the sputtering power is fixed at 1200 W.

The sputtering rate has a very prominent linear dependence on the deposition power and is only slightly affected by the chamber pressure within the investigated region [Fig. 3(a)]. The Scherrer crystallite size is found to vary significantly and it does not simply follow the adatom energy: the crystallite size increases on lowering the deposition power, which is associated with lowering adatom energies; but it also increases on lowering the Ar pressure, which is associated with higher adatom energies. The AFM data on the average grain size demonstrate a similar trend to the Scherrer crystallite size obtained with XRD. The rms roughness of all samples, obtained from  $5 \times 5 \mu\text{m}^2$  AFM scans, is also presented in Fig. 3(a).

The magnetic properties of the resulting continuous films, obtained locally using Kerr microscopy and integrating over the whole field of view, are given in Fig. 3(b) versus the average crystallite size obtained from

XRD. Both the anisotropy and coercivity of the Py films decrease simultaneously with increasing adatom energy, upon either increasing the sputtering power or lowering the chamber pressure. The thin-film resistivity, in contrast, demonstrates a linear correlation with the Scherrer crystallite size [given in Fig. 3(b) inset]. The AMR values, defined as  $\Delta R/R = 100 \frac{R_{\parallel} - R_{\perp}}{R_{\perp}}$ , are  $2.5 \pm 0.2\%$  for all measured samples. The combined effect of low inert gas pressure and high deposition power resulting in high deposition rates enables low coercivity and anisotropy values of the 30-nm-thick Py films sputtered in an RMF, down to 0.01 mT and  $18 \text{ J/m}^3$ , respectively, to be achieved, while keeping a high AMR ratio.

All samples demonstrate a small but finite anisotropy constant despite the expected disorienting effect of sputtering on the rotating substrate and in an RMF to eliminate anisotropy. Rotating magnetic fields in combination with normal incidence of material flow have been reported [32] to produce magnetically isotropic Py films. This

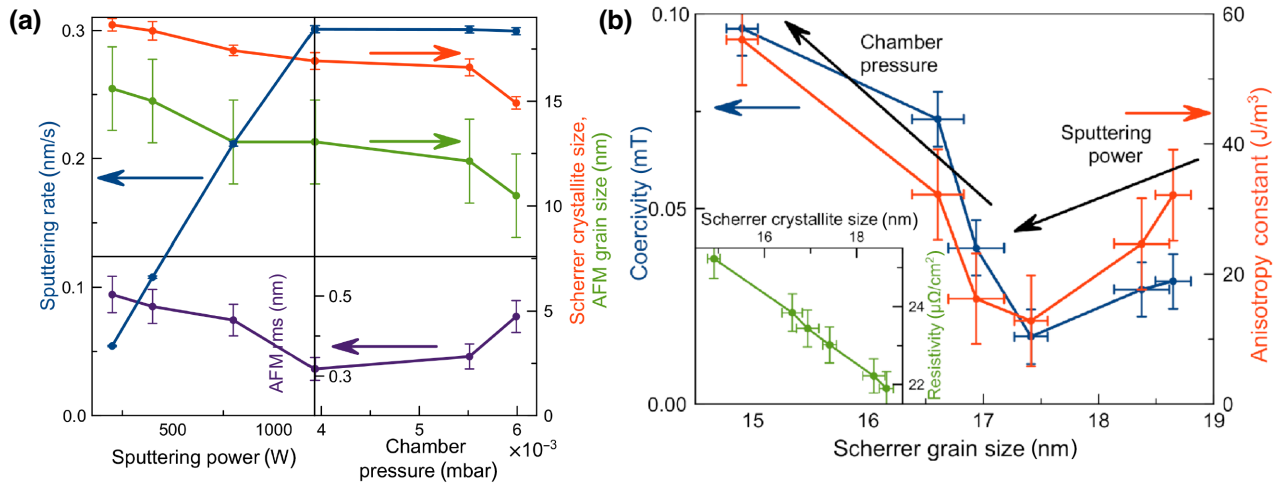


FIG. 3. (a) The sputtering rates (blue dots), Scherrer average crystallite sizes (red dots), AFM average grain sizes (green dots), and AFM RMS surface roughness (purple dots) of Py films sputtered with different powers and chamber pressures. For varied sputtering power, the chamber pressure is fixed at  $4 \times 10^{-3}$  mbar and for varied chamber pressure, the sputtering power is fixed at 1200 W. The inset shows an AFM image of the sample marked with an orange circle. (b) The coercivity (blue dots), anisotropy (red dots), and resistivity (green dots) of the continuous permalloy films as a function of the Scherrer average crystallite size for growth with a rotating magnetic field (i.e., fixed in the laboratory frame) of 5 mT.

discrepancy might be caused by utilizing the  $\text{Ni}_{47}\text{Cr}_{42}\text{Fe}_{11}$  seed layer, a tilted sputtering target orientation, or a different method and/or spatial resolution for determining the magnetic properties compared to the cited paper.

Sets of Py-film samples sputtered in the absence of a magnetic field (zero magnetic field, ZMF), in a suppressing magnetic field (an RMF), or in an AMF (a static magnetic field) are investigated by means of both local Kerr microscopy and integral VSM averaging over the whole sample. The local Kerr measurements demonstrate a finite anisotropy for a ZMF and an RMF with random values and orientations when measured at different spots in the samples. Figure 4(a) presents remanence magnetization loops obtained for the RMF sample (sputtered at a power of 1200 W and a pressure of  $P_{\text{Ar}} = 5.5 \times 10^{-3}$  mbar) at different spots; similar behavior is observed in the case of the ZMF sample, while the AMF sample exhibits uniform values of anisotropy and coercivity all over the sample (the ZMF and AMF samples are not shown). The local magnetic parameters measured at different spots in the continuous films vary in both the direction and value of the anisotropy, while the easy-axis coercivity remains approximately constant.

The VSM results underline these differences [Fig. 4(b)]: the hysteresis curves on the AMF sample demonstrate high squareness in the easy direction and a zero-coercivity loop in the hard direction. The RMF sample demonstrates zero averaged-out anisotropy and the ZMF sample still demonstrates low but finite anisotropy.

Variation of the strength of the external magnetic field applied during sputtering with the other parameters fixed (chamber pressure  $5.5 \times 10^{-3}$  mbar, sputtering power 1200 W, substrate rotation 1 Hz) results in collective

change of the coercivity and anisotropy, as shown in Fig. 4(c). Small magnetic fields of about 1 mT already suffice to obtain the full effect of the RMF or AMF.

Switching of the continuous films is observed to occur via the formation of magnetization ripples (see Fig. 4(c), inset; sample sputtered at a power of 1200 W, a pressure of  $P_{\text{Ar}} = 5.5 \times 10^{-3}$  mbar, and using a ZMF), which indicates locally varying directions of the easy axis. For samples sputtered in an RMF or a ZMF, the main ripple orientation does not follow the same direction across the sample but has apparently random orientations at different probed points. This magnetic behavior of continuous films, i.e., the formation of magnetization ripples in the switching patterns of globally isotropic Py films, has been reported previously [32].

Various types of magnetic film defects can be sources of local anisotropy. To isolate sparsely distributed sources of stronger anisotropy that could be causing variations of the magnetic properties in the RMF- and ZMF-sputtered Py films, the films are patterned into arrays of disks. Measurements of the angle-resolved coercivity and remanence magnetization on the patterned samples do not exhibit any notable angular  $\frac{\pi}{3}$  periodicity, so we can exclude a significant contribution of the dipolar interaction between disks. The remanent-magnetization states and the corresponding magnetization-hysteresis curves of two samples are presented in Fig. 5 (power 1200 W, pressure  $P_{\text{Ar}} = 5.5 \times 10^{-3}$  mbar, and an AMF or an RMF).

We observe a discrepancy between the local and averaging measurements of the coercivity and anisotropy of the thin permalloy films. Patterning into disks results in obtaining uniform local data on magnetic properties, which

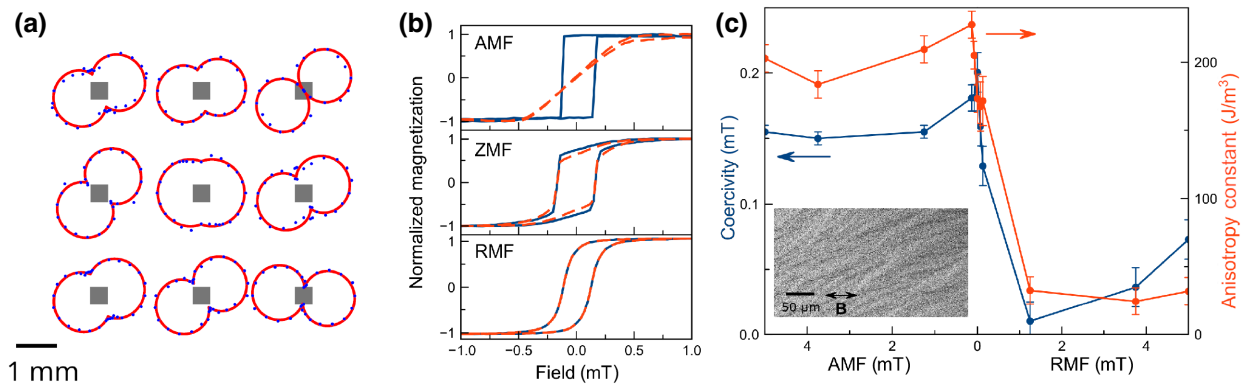


FIG. 4. The influence of aligning (AMF), rotating (RMF), or zero magnetic (ZMF) fields applied during film deposition on the magnetic properties of the continuous films. (a) Normalized polar plots of the remanence magnetization versus the angle of the field applied during measurement for an RMF (blue dots) and their fits using the modified Stoner-Wohlfarth model (red curves). The gray squares sketch out the size and relative positions of the areas on the continuous permalloy film that are probed by Kerr microscopy. (b) Hysteresis loops obtained by VSM for AMF, RMF, and ZMF films. The easy-axis loops are shown in blue and the hard-axis loops in red. (c) The easy-axis coercivity (blue dots) and anisotropy constant (red dots) versus the applied magnetic field strength for AMF and RMF geometries as measured by Kerr microscopy. The inset shows the remanent-magnetization pattern of the ZMF-sputtered Py film; the indicated external magnetic field direction **B** coincides with the sensitive orientation of the magnetic contrast in the Kerr microscope for all measurements.

agrees with the data recorded with averaging methods from a disk array. The choice of averaging over many permalloy disks improves the signal-to-noise ratio. Measuring

single disks free from the mentioned defects multiple times and averaging out over separate measurements results in similar hysteresis curves as for averaging over multiple

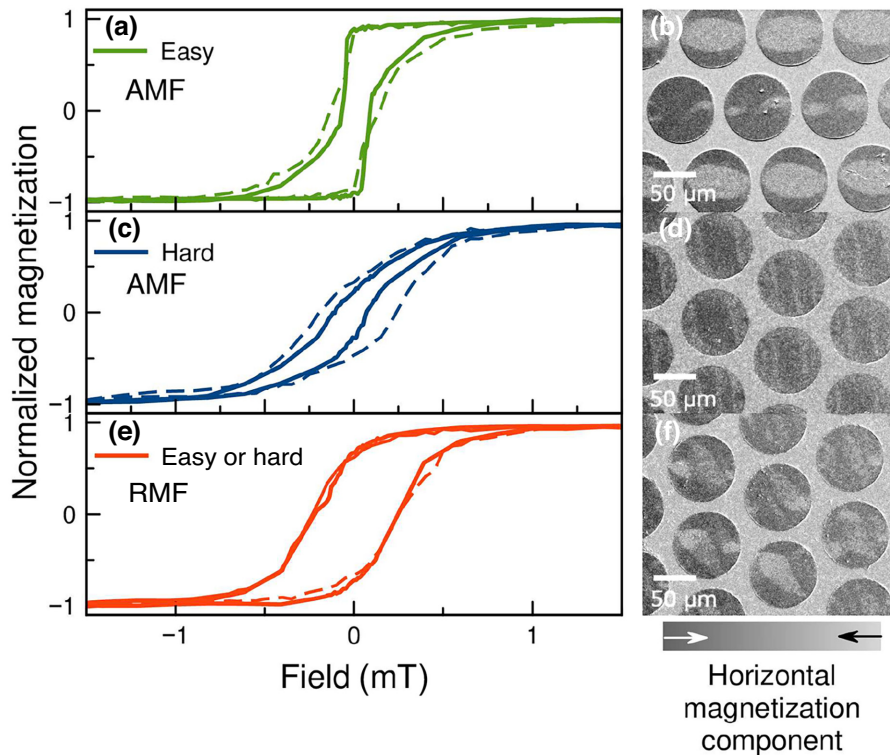


FIG. 5. Magnetic hysteresis loops and the corresponding remanent-magnetization configurations, illustrating the switching mechanisms of the patterned permalloy samples deposited in (a)–(d) an AMF [(a),(b) represent switching along the easy axis and (c),(d) along the hard axis] and (e),(f) an RMF. The solid lines represent local measurements integrated over the given field of view from Kerr microscopy and the dashed lines give integral values obtained from the whole pattern with VSM.

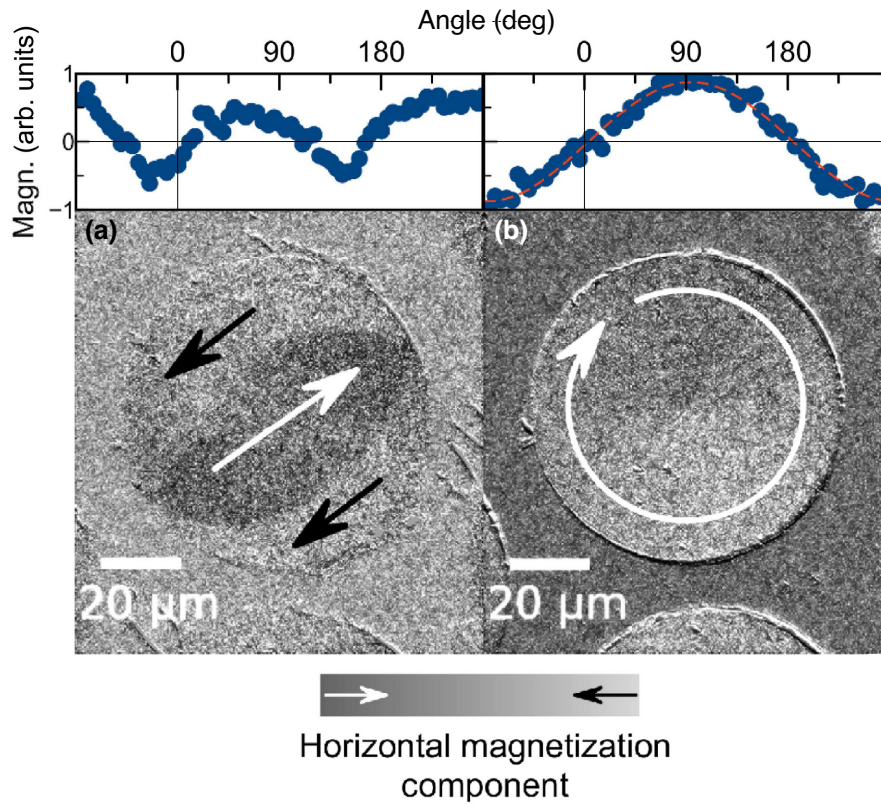


FIG. 6. Characteristic magnetization configurations of demagnetized permalloy disks from Kerr microscopy images: (a) the  $S$  state for AMF samples and (b) the symmetric vortex state for RMF samples and the corresponding averaged intensities in a disk sector as functions of their polar angles.

disks, as long as the individual disk does not carry a defect.

Compared to the continuous-film results, the patterned AMF samples retain their easy-axis directions but the easy-axis hysteresis loops become less square and the hard-axis loops exhibit a higher coercivity when patterned into disks. The hysteresis curves of RMF samples show higher coercivities in all in-plane directions and a completely vanishing anisotropy, which indicates that applying an RMF is an effective strategy to further optimize the permalloy properties (Fig. 5).

The magnetic states of demagnetized disks of the presented samples are also qualitatively different: AMF permalloy disks tend to form  $S$  states [53] where the magnetization is predominantly aligned with the easy axis, while RMF disks form single vortices with a circular magnetization distribution (Fig. 6). For demagnetizing, a gradually decreasing alternating magnetic field is applied in the horizontal direction.

#### IV. DISCUSSION

The deposition method, the fcc crystal lattice, and the use of the Ni-Cr-Fe underlayer tend to form textured films with a columnar structure, with the grain size in the  $z$

direction being close to the film thickness [54]. Figure 3(a) demonstrates a significant discrepancy between the XRD and AFM results. The AFM data are only recording the grain-size distribution in the  $x$ - $y$  plane, which explains the systematically smaller values compared to the Scherrer analysis of the XRD results that implies a spherical shape of the Py crystallites, while in reality they are extended along the growth direction. The observed decrease of the electrical resistivity with increasing grain size that is presented in Fig. 3(b) is the expected behavior [55] and it supports the performed analysis of the crystallite sizes from the Scherrer data given in Fig. 3(a). The rms roughness of all samples, obtained from  $5 \times 5 \mu\text{m}^2$  AFM scans, is around 0.4 nm. Its value decreases slightly toward higher sputtering powers and increases again with increasing chamber pressure, thus consistently following the inverse trend of the adatom energy [10].

With all of the above said, Fig. 3(b) demonstrates a distinctive nonmonotonic dependence of the coercivity and anisotropy of the permalloy films on their average crystallite size. The coercivity of thin permalloy films is generally reported to show a monotonous increase with the film thickness and crystallite size for thicknesses above 5 nm [56,57]. This grain coarsening is caused by Ostwald ripening during deposition at high temperatures and is

accompanied by a substantial increase in surface roughness [57].

A higher sputter power and a lower chamber pressure both increase the adatom energy. Higher adatom energies at lower chamber pressure result in smoother and denser films due to the incorporation of excess atoms in the film causing compressive stress [46] and reducing the coercivity. The same qualitative behavior is also in agreement with the structure-zone model [54] for sputtering, as introduced by Thornton [58]. Decreasing the chamber pressure at fixed high sputter power leads to a transition from the so-called “Zone 1” into the transitional “Zone T,” which is accompanied by an increase in grain size. No significant changes in density or roughness of the sputtered films are observed by XRR but minor changes of density and roughness can already give rise to significant changes of coercivity.

However, while the chamber pressure has almost no effect on the deposition rate [Fig. 3(a)], the deposition rate changes in proportion to the sputter power. Changing the sputter power has two effects: while the increased adatom energy still favors larger grains by stronger self-annealing, the increased deposition rate leads to a stronger nucleation (magnetron sputtering of metals starts according to the Volmer-Weber mechanism [59]), resulting in smaller grains, which appears to be the dominant mechanism in the studied films.

Another interesting finding is the nonzero anisotropy of the Py films sputtered onto the rotating substrate in ZMF conditions (Fig. 4). This provides additional insight into the counterplay of the aligning abilities of the tilted target and the external magnetic field. Previous studies have demonstrated that without substrate rotation, an RMF during deposition results in isotropic Py films only for a normal target position, while target tilt results in a uniaxial anisotropy, where the direction and magnitude are defined by the tilt angle [32]. Another study has concluded that deposition in a static external magnetic field using a tilted target with perpendicular (competing) directions results in a target-tilt-defined anisotropy direction [60]. In our experiment, the aligning effect of the magnetic field prevails over the disorientation caused by the target tilt, resulting in a well-defined uniaxial anisotropy (Fig. 4(a), AMF sample). Globally isotropic films are only produced by the joint disorienting effect of a rotating molecular beam and magnetic field (Fig. 4(a), RMF sample).

The microscopic study of the magnetic properties of the samples sputtered in an RMF or a ZMF demonstrates that within a single field of view, significantly varying anisotropy directions and magnitudes coexist. The varying anisotropy directions and magnitudes demonstrated in Fig. 4(a) cannot be explained by a simple permalloy texture or strain that is uniform across the sample; nor can they be explained by an influence from the edges of the film, which would result in a symmetric distribution.

Another source of random anisotropy can be the presence of residual magnetic material on the sample holder. We cannot confirm this mechanism for our system, as the use of a pristine sample holder gives comparable results for ZMF deposition. However, it is reasonable to assume that the effect of residual magnetic material on the sample holder can also be overcome by choosing sufficiently high magnetic field strengths of the AMF or RMF growth, as then any magnetic fields from residual material are insignificant compared to the externally applied field. One of the possible explanations concerns random irregularities of the substrate during growth (dust particles, scratches, or randomly formed magnetization clusters or voids) orienting the soft Py in an extended surrounding region. Since Py is a very soft magnetic material, such defects can also serve as domain-wall nucleation sites [57] dominating the switching properties of the film and leading to spatially varying properties. In this case, the integral measurements are not necessarily representative of the intrinsic properties of the Py but, rather, they simply probe such random imperfections.

Samples grown by thermal evaporation provide an additional insight into the formation of areas of random anisotropy in Py films. For comparison, we deposit two Py films by thermal evaporation without sample or field rotation in a different UHV deposition chamber, where the sample temperature can be varied. The anisotropy of the Py film deposited on a substrate that is cooled down to liquid-nitrogen temperatures is uniform across the sample and is governed by the tilt of the Py source with respect to the substrate plane. The sample deposited at room temperature with the same source position shows random anisotropy directions and values in different probed areas. The thermal activation during growth at room temperature is already enough to overcome the source-tilt effect and self-anneal the Py film around random defects [61].

In order to isolate single sparsely distributed defects affecting the permalloy properties over an extended range and to remove the dominance of the defect contributions on the measurement results, the continuous-film samples are patterned into arrays of disks. The disk radii are chosen to be smaller than the area of uniform ripple orientation but much larger than the permalloy exchange length, the spacing being large enough to avoid interaction with neighboring disks. Square packaging might be a source of biaxial anisotropy due to the interaction between neighboring disks, so we choose a hexagonal arrangement, which also improves the signal-to-noise ratio of the MOKE measurements. In the case of patterned films, the magnetization reversal is governed by the more homogeneous local material parameters as well as by the reduction of stray field energy orienting the magnetic moments along the edges of the disks.

The shape of the hysteresis loops observed for the patterned AMF samples along the easy-axis direction is



typical of disk-patterned samples [62] and is caused by the formation of  $S$  states. Switching along the hard axis occurs through the formation of elongated parallel domains confined by the disk size and results in an increased coercivity of the hysteresis loops. Switching in the RMF samples also takes place through the formation of multidomain states; however, they are more complex and show more variation (Fig. 5). The magnetic state of the horizontally demagnetized disks of RMF Py is a symmetric vortex that is the ground state in the disks in the absence of anisotropy [see Fig. 6(b); the averaged intensity in a disk sector as a function of its polar angle yields a sine curve]. In contrast, the magnetization of the AMF disks reflects the interplay between the introduced anisotropy and the reduction of stray field energy at the edge of the disks, resulting in  $S$  states [Fig. 6(a)]. The employment of this approach to the study of samples exposed to an AMF or an RMF during deposition provides two observations. First, the AMF results in Py films with uniform magnetic properties and a defined anisotropy direction, despite the disorienting effects of the target tilt caused by substrate rotation. Second, patterning of the RMF samples isolates major defects, suppresses the magnetization ripple formation and, on the smaller scale, the permalloy films demonstrate isotropic magnetic properties.

## V. CONCLUSIONS

In conclusion, we investigate the effect of varied magnetron sputtering conditions on the magnetic properties of Py, in order to obtain soft magnetic isotropic thin films. The best samples with the lowest coercivity (down to 0.01 mT) and vanishing average anisotropy are obtained using higher sputtering powers (1200 W) and low Ar pressures ( $4 \times 10^{-3}$  mbar). The above-discussed approaches are found to improve the magnetic properties of Py by affecting the crystallite size and have been reported to lead to the formation of denser and smoother films [46]. They can, in turn, be combined with the reported AMR enhancement obtained by introducing various seed layers (Ni-Cr-Fe [48], Pt [63], or Co-Fe-B [64]) to improve the performance of various AMR-based devices. We observe a local variation of the magnetic properties of continuous Py films despite the disorienting effects of sample rotation with respect to the target tilt and the rotating external magnetic field. The patterning of such films into arrays of disks suppresses this variation, which suggests a dominant long-range influence of random defects that affect the magnetic properties of the films in the unpatterned samples. Thus, the investigation of patterned samples provides a general and robust approach to investigate the intrinsic film properties, which can then be unambiguously related to variations in deposition conditions.

## ACKNOWLEDGMENTS

This work was funded by the European Regional Development Fund (EFRE) and the Federal State of Rhineland-Palatinate under Project No. 84002616. Additional financial support was provided by the German Research Foundation (DFG) (SFB TRR 173 Spin+X, Grant No. 268565370, projects A01 and B02). This project has received funding from the European Research Council (ERC) under the European Union's Horizon 2020 research and innovation program via Synergy Grant No. 856538 (project "3D MAGiC") and Marie Skłodowska-Curie Grant No. 860060 "Magnetism and the effect of Electric Field" (MagnEFi). It has also received funding from the Horizon Europe Framework Programme of the European Commission under HORIZON-CL4-2021-DIGITAL-EMERGING-01 Grant Agreement No. 101070290 (NIMFEIA). A.P.B. acknowledges the Alexander von Humboldt Foundation for a postdoctoral fellowship (Grant Ref. 3.5-IND-1216986-HFST-P). We are grateful to Analog Devices for additional funding and support within a joint research project.

- 
- [1] K. Barmak and K. Coffey, *Metallic Films for Electronic, Optical and Magnetic Applications: Structure, Processing and Properties* (Woodhead Publishing, Sawston, Cambridge, UK, 2014).
  - [2] A. García-Arribas, E. Fernández, A. V. Svalov, G. V. Kurlyandskaya, A. Barrainkua, D. Navas, and J. M. Barandiaran, Tailoring the magnetic anisotropy of thin film permalloy microstrips by combined shape and induced anisotropies, *Eur. Phys. J. B* **86**, 1 (2013).
  - [3] E. B. Park, S.-U. Jang, J.-H. Kim, and S.-J. Kwon, Induced magnetic anisotropy and strain in permalloy films deposited under magnetic field, *Thin Solid Films* **520**, 5981 (2012).
  - [4] B. Borie, J. Wahrhusen, H. Grimm, and M. Kläui, Geometrically enhanced closed-loop multi-turn sensor devices that enable reliable magnetic domain wall motion, *Appl. Phys. Lett.* **111**, 242402 (2017).
  - [5] D. A. Allwood, G. Xiong, C. Faulkner, D. Atkinson, D. Petit, and R. Cowburn, Magnetic domain-wall logic, *Science* **309**, 1688 (2005).
  - [6] J. Wang, X. Zhang, X. Lu, J. Zhang, Y. Yan, H. Ling, J. Wu, Y. Zhou, and Y. Xu, Magnetic domain wall engineering in a nanoscale permalloy junction, *Appl. Phys. Lett.* **111**, 072401 (2017).
  - [7] L. Romankiw, I. Croll, and M. Hatzakis, Batch-fabricated thin-film magnetic recording heads, *IEEE Trans. Magn.* **6**, 597 (1970).
  - [8] M. Kläui, Head-to-head domain walls in magnetic nanostructures, *J. Phys.: Condens. Matter* **20**, 313001 (2008).
  - [9] S. S. Parkin, M. Hayashi, and L. Thomas, Magnetic domain-wall racetrack memory, *Science* **320**, 190 (2008).
  - [10] H. Seet, X. Li, J. Yi, W. Ooi, and K. Lee, Effect of deposition methods on the magnetic properties of nanocrystalline permalloy, *J. Alloys Compd.* **449**, 284 (2008).

- [11] S. Andreev and P. Dimitrova, Anisotropic-magnetoresistance integrated sensors, *J. Optoelectron. Adv. Mater.* **7**, 199 (2005).
- [12] Z. Wang, X. Wang, M. Li, Y. Gao, Z. Hu, T. Nan, X. Liang, H. Chen, J. Yang, and S. Cash, *et al.*, Highly sensitive flexible magnetic sensor based on anisotropic magnetoresistance effect, *Adv. Mater.* **28**, 9370 (2016).
- [13] T. Iwata and F. Hagedorn, Annealing behavior of induced anisotropy and related magnetic properties in permalloy films, *J. Appl. Phys.* **40**, 2258 (1969).
- [14] D. O. Smith, Anisotropy in permalloy films, *J. Appl. Phys.* **30**, S264 (1959).
- [15] M. Kateb, H. Hajihoseini, J. T. Gudmundsson, and S. Ingvarsson, Comparison of magnetic and structural properties of permalloy Ni<sub>80</sub>Fe<sub>20</sub> grown by dc and high power impulse magnetron sputtering, *J. Phys. D: Appl. Phys.* **51**, 285005 (2018).
- [16] M. Sultan, Effect of gas pressure and flow rate on the plasma power and deposition rate in magnetron sputtering system, *Res. J. Nanosci. Eng* **2**, 1 (2018).
- [17] J. Wei, Z. Zhu, C. Song, H. Feng, P. Jing, X. Wang, Q. Liu, and J. Wang, Annealing influence on the exchange stiffness constant of permalloy films with stripe domains, *J. Phys. D: Appl. Phys.* **49**, 265002 (2016).
- [18] C. Luo, Z. Feng, Y. Fu, W. Zhang, P. Wong, Z. Kou, Y. Zhai, H. Ding, M. Farle, and J. Du, *et al.*, Enhancement of magnetization damping coefficient of permalloy thin films with dilute Nd dopants, *Phys. Rev. B* **89**, 184412 (2014).
- [19] Q. Chen, Y. Yin, H. Yuan, X. Zhou, Z. Huang, J. Du, and Y. Zhai, Effect of dilute rare-earth doping on magnetodynamic properties of permalloy films, *IEEE Magn. Lett.* **10**, 1 (2019).
- [20] S. Mizukami, T. Kubota, X. Zhang, H. Naganuma, M. Oogane, Y. Ando, and T. Miyazaki, Influence of Pt doping on Gilbert damping in permalloy films and comparison with the perpendicularly magnetized alloy films, *Jpn. J. Appl. Phys.* **50**, 103003 (2011).
- [21] R. Bozorth, The permalloy problem, *Rev. Mod. Phys.* **25**, 42 (1953).
- [22] L. Yin, D. Wei, N. Lei, L. Zhou, C. Tian, G. Dong, X. Jin, L. Guo, Q. Jia, and R. Wu, Magnetocrystalline Anisotropy in Permalloy Revisited, *Phys. Rev. Lett.* **97**, 067203 (2006).
- [23] J. Han-Min, C.-O. Kim, T.-D. Lee, and H.-J. Kim, Origin of magnetization-induced anisotropy of magnetic films, *Chin. Phys.* **16**, 3520 (2007).
- [24] J. Rantschler, R. McMichael, A. Castillo, A. Shapiro, W. Egelhoff Jr, B. Maranville, D. Pulgurtha, A. Chen, and L. Connors, Effect of 3*d*, 4*d*, and 5*d* transition metal doping on damping in permalloy thin films, *J. Appl. Phys.* **101**, 033911 (2007).
- [25] W. Bailey, P. Kabos, F. Mancoff, and S. Russek, *et al.*, Control of magnetization dynamics in Ni<sub>81</sub>Fe<sub>19</sub> thin films through the use of rare-earth dopants, *IEEE Trans. Magn.* **37**, 1749 (2001).
- [26] J. Beik Mohammadi, G. Mankey, C. K. Mewes, and T. Mewes, Strong interfacial perpendicular anisotropy and interfacial damping in Ni<sub>0.8</sub>Fe<sub>0.2</sub> films adjacent to Ru and SiO<sub>2</sub>, *J. Appl. Phys.* **125**, 023901 (2019).
- [27] Y. Zhao, Q. Song, S.-H. Yang, T. Su, W. Yuan, S. S. Parkin, J. Shi, and W. Han, Experimental investigation of temperature-dependent Gilbert damping in permalloy thin films, *Sci. Rep.* **6**, 1 (2016).
- [28] S. Kezilebieke, M. Ali, B. Shadeke, and R. Gunnella, Magnetic properties of ultrathin Ni<sub>81</sub>Fe<sub>19</sub> films with Ta and Ru capping layers, *J. Phys.: Condens. Matter* **25**, 476003 (2013).
- [29] M. Kowalewski, W. Butler, N. Moghadam, G. Stocks, T. Schulthess, K. Song, J. Thompson, A. Arrott, T. Zhu, and J. Drewes, *et al.*, The effect of Ta on the magnetic thickness of permalloy (Ni<sub>81</sub>Fe<sub>19</sub>) films, *J. Appl. Phys.* **87**, 5732 (2000).
- [30] T. McGuire and R. Potter, Anisotropic magnetoresistance in ferromagnetic 3d alloys, *IEEE Trans. Magn.* **11**, 1018 (1975).
- [31] A. Kavitha, R. Kannan, and S. Rajashabala, Effect of target power on the physical properties of Ti thin films prepared by dc magnetron sputtering with supported discharge, *Mater. Sci. Poland* **35**, 173 (2017).
- [32] E. Fuchs and W. Zinn, Isotropic permalloy films, *J. Appl. Phys.* **34**, 2557 (1963).
- [33] M. Kateb, E. Jacobsen, and S. Ingvarsson, Application of an extended van der Pauw method to anisotropic magnetoresistance measurements of ferromagnetic films, *J. Phys. D: Appl. Phys.* **52**, 075002 (2018).
- [34] R. Prosen, B. Gran, J. Kivel, C. Searle, and A. Morrish, Effect of surface roughness on magnetic properties of films, *J. Appl. Phys.* **34**, 1147 (1963).
- [35] J. Berendt, J. Teixeira, A. García-García, M. Raposo, P. Ribeiro, J. Dubowik, G. Kakazei, and D. Schmool, Tunable magnetic anisotropy in permalloy thin films grown on holographic relief gratings, *Appl. Phys. Lett.* **104**, 082408 (2014).
- [36] X. Li, X. Sun, J. Wang, and Q. Liu, Magnetic properties of permalloy films with different thicknesses deposited onto obliquely sputtered Cu underlayers, *J. Magn. Magn. Mater.* **377**, 142 (2015).
- [37] L. McKeehan, Magnetic interaction and resultant anisotropy in unstrained ferromagnetic crystals, *Phys. Rev.* **52**, 18 (1937).
- [38] D. C. Rodrigues, A. B. Klautau, A. Edström, J. Ruzs, L. Nordström, M. Pereiro, B. Hjörvarsson, and O. Eriksson, Magnetic anisotropy in permalloy: Hidden quantum mechanical features, *Phys. Rev. B* **97**, 224402 (2018).
- [39] S. Chikazumi, Ferromagnetic properties and superlattice formation of iron nickel alloys (i), *J. Phys. Soc. Jpn.* **5**, 327 (1950).
- [40] J. Slonczewski, Induced anisotropy in Ni-Fe films, *IEEE Trans. Magn.* **4**, 15 (1968).
- [41] C. Wilts and F. Humphrey, Magnetic anisotropy in flat ferromagnetic films: A review, *J. Appl. Phys.* **39**, 1191 (1968).
- [42] M. Kateb and S. Ingvarsson, Correlation of uniaxial magnetic anisotropy axes and principal resistivities in polycrystalline ferromagnetic films, *J. Magn. Magn. Mater.* **532**, 167982 (2021).
- [43] W. Andrä, Z. Málek, W. Schüppel, and O. Stemme, “Spontaneous magnetic anisotropy” in polycrystalline thin films, *J. Appl. Phys.* **31**, 442 (1960).
- [44] K. J. Harte, Theory of large-angle ripple in magnetic films, *J. Appl. Phys.* **37**, 1295 (1966).

- [45] R. Alben, J. Becker, and M. Chi, Random anisotropy in amorphous ferromagnets, *J. Appl. Phys.* **49**, 1653 (1978).
- [46] C. V. Thompson, Structure evolution during processing of polycrystalline films, *Annu. Rev. Mater. Sci.* **30**, 159 (2000).
- [47] K. Chan and B. Teo, Effect of Ar pressure on grain size of magnetron sputter-deposited Cu thin films, *IET Sci., Meas. Technol.* **1**, 87 (2007).
- [48] W. Lee, M. Toney, and D. Mauri, High magnetoresistance in sputtered permalloy thin films through growth on seed layers of  $(\text{Ni}_{0.81}\text{Fe}_{0.19})_{1-x}\text{Cr}_x$ , *IEEE Trans. Magn.* **36**, 381 (2000).
- [49] P. Solovev, A. Izotov, and B. Belyaev, Microstructural and magnetic properties of thin obliquely deposited films: A simulation approach, *J. Magn. Magn. Mater.* **429**, 45 (2017).
- [50] M. Johnson, P. Bloemen, F. Den Broeder, and J. De Vries, Magnetic anisotropy in metallic multilayers, *Rep. Prog. Phys.* **59**, 1409 (1996).
- [51] M. Dumm, M. Zöfl, R. Moosbühler, M. Brockmann, T. Schmidt, and G. Bayreuther, Magnetism of ultrathin FeCo (001) films on GaAs (001), *J. Appl. Phys.* **87**, 5457 (2000).
- [52] K. Wang, Y. Huang, R. Chen, and Z. Xu, Investigation of magnetic properties in thick CoFeB alloy films for controllable anisotropy, *Appl. Phys. A* **122**, 1 (2016).
- [53] M. Schneider, H. Hoffmann, S. Otto, T. Haug, and J. Zweck, Stability of magnetic vortices in flat submicron permalloy cylinders, *J. Appl. Phys.* **92**, 1466 (2002).
- [54] E. Kusano, Structure-zone modeling of sputter-deposited thin films: A brief review, *Appl. Sci. Converg. Technol.* **28**, 179 (2019).
- [55] A. Mayadas, J. Janak, and A. Gangulee, Resistivity of permalloy thin films, *J. Appl. Phys.* **45**, 2780 (1974).
- [56] M. Akhter, D. Mapps, Y. Ma Tan, A. Petford-Long, and R. Doole, Thickness and grain-size dependence of the coercivity in permalloy thin films, *J. Appl. Phys.* **81**, 4122 (1997).
- [57] N. Djuzhev, A. Iurov, N. Mazurkin, M. Chinenkov, A. Trifonov, and M. Pushkina, in *EPJ Web of Conferences*, Vol. 185 (EDP Sciences, 2018), p. 01003.
- [58] J. A. Thornton, The microstructure of sputter-deposited coatings, *J. Vac. Sci. Technol. A: Vac., Surf., Films* **4**, 3059 (1986).
- [59] N. Kaiser, Review of the fundamentals of thin-film growth, *Appl. Opt.* **41**, 3053 (2002).
- [60] M. Kateb and S. Ingvarsson, in *2017 IEEE Sensors Applications Symposium (SAS)* (IEEE, 2017), p. 1.
- [61] R. M. Bozorth, *et al.*, *Magnetic Properties of Metals and Alloys* (American Society for Metals, Cleveland, Ohio, 1959).
- [62] R. Ferrero, A. Manzin, G. Barrera, F. Celegato, M. Coisson, and P. Tiberto, Influence of shape, size and magnetostatic interactions on the hyperthermia properties of permalloy nanostructures, *Sci. Rep.* **9**, 1 (2019).
- [63] Y. Liu, J. Cai, and L. Sun, Large enhancement of anisotropic magnetoresistance and thermal stability in Ta/NiFe/Ta trilayers with interfacial Pt addition, *Appl. Phys. Lett.* **96**, 092509 (2010).
- [64] M. Li, H. Shi, Y. Dong, L. Ding, G. Han, Y. Zhang, Y. Liu, and G. Yu, Effect of a CoFeB layer on the anisotropic magnetoresistance of Ta/CoFeB/MgO/NiFe/MgO/CoFeB/Ta films, *J. Magn. Magn. Mater.* **439**, 17 (2017).